Solar Phys (2010) 267: 343–359
DOI 10.1007/s11207-010-9648-7

Radio Observations of the 20 January 2005 X-class Flare

C. Bouratzis · P. Preka-Papadema · A. Hillaris · P. Tsitsipis · A. Kontogeorgos · V.G. Kurt · X. Moussas

Received: 8 December 2009 / Accepted: 28 September 2010 / Published online: 2 November 2010

Abstract We present a multi-frequency and multi-instrument study of the 20 January 2005 event. We focus mainly on the complex radio signatures and their association with the active phenomena taking place: flares, CMEs, particle acceleration, and magnetic restructuring. As a variety of energetic-particle accelerators and sources of radio bursts are present, in the flare – ejecta combination, we investigate their relative importance in the progress of this event. The dynamic spectra of ARTEMIS-IV – *Wind*/*Waves* – HiRAS, with 2000 MHz – 20 kHz frequency coverage, were used to track the evolution of the event from the low corona to the interplanetary space; these were supplemented with SXR, HXR, and γ-ray recordings. The observations were compared with the expected radio signatures and energetic-particle populations envisaged by the *Standard Flare – CME model* and the *recon-*

C. Bouratzis · P. Preka-Papadema · A. Hillaris (✉) · X. Moussas
Section of Astrophysics, Astronomy and Mechanics, Department of Physics, University of Athens, Zografos (Athens), 15783, Greece
e-mail: ahilaris@phys.uoa.gr

C. Bouratzis
e-mail: kbouratz@phys.uoa.gr

P. Preka-Papadema
e-mail: ppreka@phys.uoa.gr

X. Moussas
e-mail: xmoussas@phys.uoa.gr

P. Tsitsipis · A. Kontogeorgos
Department of Electronics, Technological Educational Institute of Lamia, Lamia, 35100, Greece

P. Tsitsipis
e-mail: tsitsipis@teilam.gr

A. Kontogeorgos
e-mail: akontog@teilam.gr

V.G. Kurt
Skobeltsyn Institute of Nuclear Physics, Lomonosov Moscow State University, Moscow, 119992, Russia
e-mail: vgk@srd.sinp.msu.ru

nection outflow termination shock model. A proper combination of these mechanisms seems to provide an adequate model for the interpretation of the observational data.

Keywords Radio bursts · Dynamic spectrum · Type III · Type II · Type IV

1. Introduction

Solar flares and coronal mass ejections (CMEs) are the most energetic phenomena on the Sun. They can be envisaged as two different aspects of a common magnetic energy instability and release (see, *e.g.*, Pick *et al.*, 2006, and references therein), described by the standard CME – flare model, which combines the kinematics of the energy release of ejecta and flares. As the rising CME (or erupting filament or rising plasmoid) stretches and deforms the coronal magnetic-field lines, a vertical current sheet is formed, where reconnection explosively releases the free magnetic energy, stored in the corona (see *e.g.* Forbes and Lin, 2000; Forbes, 2003; Priest and Forbes, 2002); furthermore, CME acceleration profile and flare energy release are seen to evolve in a synchronized manner (Temmer *et al.*, 2010). The energy, thus liberated, is divided over plasma heating, particle acceleration, kinetic energy of the eruption, and MHD shock waves.

The development, in the low corona, of large flare/CME events coincides with an extended opening of the magnetic field, accompanied by energetic-particle acceleration and injection into interplanetary space and shocks. These are detectable, at metric and longer waves, by their radio signatures (see, *e.g.*, review by Pick and Vilmer, 2008).

The Type III burst radio emission is produced by non-thermal electrons streaming along coronal magnetic lines. In open field lines, they may escape into interplanetary space and may be detected *in situ* (see, *e.g.*, Faindberg and Stone, 1970; Lin, Evans, and Fainberg, 1973; Kurt, Logachev, and Pissarenko, 1977; Klein *et al.*, 2008). In closed magnetic structures, on the other hand, they eventually turn Sunwards, resulting in inverted U- or J-shaped bursts on the dynamic spectra (U or J bursts). Metric bursts of the Type III family generally consist of groups of individual bursts (see *e.g.* Goldman, 1983, and references within); on the reports they are marked as III G for fewer than ten occurrences and III GG for more.

The Type II bursts trace the propagation of MHD shocks in the corona and interplanetary space. It is, in general, accepted that Type II bursts at decametre and longer wavelengths are driven by CMEs, bow or flank (see, *e.g.*, Vršnak and Cliver, 2008, for a review). The Type II bursts at metre wavelengths, however, are interpreted either as a flare blast wave (Vršnak, Magdalenić, and Aurass, 2001) or as a CME-driven shock (Kahler *et al.*, 1984; Maia *et al.*, 2000; Claßen and Aurass, 2002). A metric stationary Type II burst (a Type II burst with a very slow drift on the dynamic spectrum) has been identified, for the first time, by Aurass, Vršnak, and Mann (2002); it was interpreted as the radio signature of fast-mode termination shocks by Aurass *et al.* (2006). The proposed formation process included a pair of counterstreaming outflow jets moving upwards and downwards from the reconnection site, encountering the rear of the CME and the top of the post-flare loop, respectively, resulting in termination shocks (Mann, Aurass, and Warmuth, 2006; Mann, Warmuth, and Aurass, 2009; Warmuth, Mann, and Aurass, 2009).

The continua during periods of activity represent the radiation of energetic electrons trapped within magnetic structures and plasmoids, and they are known under the names of Type IV bursts and "Flare Continua" (Robinson, 1978a, 1985). The stationary Type IV (IV mB) bursts emanate from magnetic structures usually located above active regions; they often exhibit significant fine structure. The moving Type IV bursts (Robinson, 1978b)

(IV mA) are emitted from sources of metre-wave continuum moving outwards at velocities of the order of $100-1000\ \mathrm{km\,s^{-1}}$; their spectrum is often featureless and sometimes lasts more than ten minutes. A number of these are believed to originate within the dense substructures (such as erupting prominences) within the CMEs (Klein and Mouradian, 2002; Bastian *et al.*, 2001). Others appear following Type II bursts and are possibly caused by energetic electrons produced in the wake of the Type II shock. Robinson (1985) calls them flare continua II (FCII) based on the close temporal association with the Type II and classifies them in the stationary Type IV (IV mB) family with frequency drift.

Broad-band ($\Delta f/f \approx 1$) and narrow-band ($\Delta f/f < 0.1$) pulsations are, at times, considered part of the Type IV family, being interpreted as MHD oscillations in coronal loops modulating the continuum. Alternative interpretations include limit cycles of nonlinear wave–particle interactions in coronal loops or quasi-periodic particle acceleration episodes during the magnetic reconnection in a large-scale current sheet. On the dynamic spectra, the pulsations exhibit quasi-periodic behavior ($\approx 0.1-10$ Hz) and durations from seconds to minutes; some gradually drift to lower frequency in the course of the event (see, *e.g.*, reviews by Benz, 2003; Nindos and Aurass, 2007).

Another type of radio burst, which has been associated with magnetic reconnection in solar flares, is the short (≤ 0.1 second), narrow-band (some MHz) emissions known as "spikes". They appear in broad-band clusters lasting seconds to about a minute. Metric spikes at $250-500$ MHz are quite common near the starting frequency of metric Type III bursts and are thus linked with the acceleration of electron beams (Benz, 2003; Kliem *et al.*, 2003). They are considered as the signatures of accelerated particles at a highly fragmented, primary energy-release site (Nindos and Aurass, 2007). At the same time, they pinpoint the location of the reconnection and acceleration site.

A small number of solar active phenomena has been classified as "extreme events"; in these events, characteristics such as flare intensity, CME speed, and solar-energetic particle (SEP) flux are orders of magnitude larger than the rest (Crosby, 2009). Solar-energetic proton events may result in a sharp, short-duration increase in the count rate of ground-based cosmic-ray detectors, and they are dubbed ground-level enhancements (GLEs).

The extreme event of 20 January 2005 in AR 720 (N14° W61°) included a fast CME, an X7.1/2B (6:36–7:26 UT) flare, a white-light flare, hard X-rays, γ-rays (up to 300 MeV), and radio bursts in microwave to decametric frequency. It also initiated SEP and GLE, indicating a prompt proton acceleration (Kuznetsov *et al.*, 2006, 2008; Grechnev *et al.*, 2008; Simnett, 2007) with the hardest energy spectrum of Solar Cycle 23 (Bazilevskaya, 2009). The GLE, in particular, was characterized as the most intense in half a century and among the most intense in observational history (Plainaki *et al.*, 2007; Belov, 2005), second only to the GLE of 23 February 1956 (Vashenyuk, 2005).

This report on the 20 January 2005 extreme event is structured as follows: In Section 2 we describe the instrumentation and data set used in our study; this is supplemented with an algorithm for the detection and statistical analysis of quasi-linear structures embedded in complex dynamic spectra in the Appendix. The observational results are presented in Section 3; they are discussed in Section 4 and compared with models of magnetic reconnection and particle acceleration within the framework of CME-induced reconnection. Conclusions are presented in Section 5.

2. Instrumentation and Data Processing

2.1. Instruments and Data Sets

The *Appareil de Routine pour le Traitement et l'Enregistrement Magnetique de l'Information Spectral* (ARTEMIS-IV) solar radio-spectrograph (http//web.cc.uoa.gr/artemis/) operating at Thermopylae, Greece (38°49′N, 22°41′E), since 1996 (Caroubalos *et al.*, 2001; Kontogeorgos *et al.*, 2006) consists of a seven-metre parabolic antenna covering the metric range and a dipole antenna covering the decametric range. Two receivers operate in parallel, there are a sweep frequency analyzer (ASG), covering the 650 – 20 MHz range in 630 data channels at ten samples $\sec^{-1}$, and a high-sensitivity multi-channel acousto-optical analyzer (SAO), which covers the 270 – 450 MHz range in 128 channels at 100 samples $\sec^{-1}$. The broad-band, medium time resolution recordings of the ASG are used for the detection and analysis of radio emission from the base of the corona to two $R_{\odot}$, while the narrow-band, high time resolution SAO recordings are mostly used in the analysis of the fine temporal and spectral structures.

In this work we used data from the Hiraiso Radiospectrograph (HiRAS) (25 – 2500 MHz, Kondo *et al.*, 1995) to complement the ARTEMIS-IV range in the high-frequency domain.

The *Wind*/*Waves* experiment (Bougeret *et al.*, 1995) includes the RAD2 receiver, which covers the critical frequency range from 13.825 MHz ($R_{\odot}$) to 1.075 MHz (20 $R_{\odot}$). It is complemented by the RAD1 receiver (frequency range 1040 – 20 kHz), which allows us to track the evolution of the radio sources to 1 AU.

The dynamic spectra were supplemented with recordings in the 2 – 35 GHz range of the Nobeyama Radio Polarimeter (NoRP) (Nakajima *et al.*, 1985). The event was also observed in HXR and γ-rays in the 0.03 – 300 MeV range from the *Solar Neutron and Gamma* (SONG)/CORONAS-F (Kuznetsov, 2004). We used RHESSI data from (Grechnev *et al.*, 2008). The SXR data were obtained from GOES (http//www.sel.noaa.gov/ftpmenu/indices), and the kinematics of the CME came from Gopalswamy *et al.* (2005).

The times of energetic-particle release from the low corona were determined from the reports of Saiz (2005), Grechnev *et al.* (2008), Simnett (2007), and Kurt *et al.* (2010a, 2010b).

Thus, with *Wind*/*Waves* observing the interplanetary space and HiRAS with ARTEMIS-IV the high-frequency counterpart of the event (corona and lower corona), we obtain a 2000 MHz – 20 kHz frequency coverage. This, combined with the SXR, HXR, and γ-ray recordings, makes a multi-frequency and multi-instrument study of all of different aspects of the active phenomena possible, the injection of energetic particles included, comprising the 20 January 2005 event.

2.2. Coronal Density – Height Model Selection

As plasma emission depends on electron density, which in turn may be converted to coronal height using density models, we may calculate estimates for the radio source heights and speeds from the dynamic spectra. The establishment of a frequency of observation – coronal height and frequency drift rate – radial speed correspondence is affected by ambiguities introduced by the variation of the ambient medium properties. These may be the result of burst-exciter propagation within the undisturbed plasma, over-dense or under-dense structures or CME after-flows (see, *e.g.*, Pohjolainen *et al.*, 2007; Pohjolainen, Hori, and Sakurai, 2008, for a detailed discussion on model selection).

The twofold Newkirk model (Newkirk, 1961) is adequate over active regions at heights greater than 1.05 $R_{\odot}$ (frequencies lower than 300 MHz) (Figure 4 in Wild, Smerd, and Weiss, 1963), and it is used throughout this article.

3. Association of Active Phenomena with Radio Bursts

3.1. Overview

The complex radio bursts of the extreme event of 20 January 2005 have attracted considerable attention (see, *e.g.*, Pohjolainen *et al.*, 2007; Masson *et al.*, 2009; Grechnev *et al.*, 2008; Mavromichalaki, 2009).

The metric-radio-burst complex includes two distinct metric – decametric Type II (6:39 – 06:58 UT), in close succession, each associated in time with a flare-continuum-like burst (FCII), and Type III activity both isolated and in large groups (III GG). These are superposed on an extended (06:36 UT to well past 08:00 UT) Type IV continuum with rich fine structure (mostly fibers and pulsations). In the decametric frequency range, a stationary shock (with almost no drift) appears in the 40 (F) and 80 (H) MHz bands from 06:45:12 UT to 07:02'UT.

The radio bursts were accompanied by GOES/SXR and HXR, γ-ray emission in the 0.03 – 300 MeV range from SONG/CORONAS-F, and RHESSI; the high-energy channels exhibit a sharp rise of intensity at 06:45:30 UT (Kuznetsov *et al.*, 2008; Grechnev *et al.*, 2008; Masson *et al.*, 2009).

Small time-scale, narrow-band features were recorded at high resolution by ARTEMIS-IV/SAO, as part of the Type IV and FCII fine structures. The latter provide evidence of magnetic reconnection and electron acceleration in AR 720 (N14° W61°).

An overview of the time sequence of the observations used in this report is presented in Table 1. In Figure 1 we present a combined dynamic spectrum of the radio bursts; we have included the CME trajectory, the GOES SXR and SONG 40 – 100 KeV light curves, and the times of energetic-particle injections for comparison. Details of the Type II events (II(1), II(2) and II(4)) are presented in Figures 2 and 4.

In the following subsections, we have partitioned our description of the event, and the corresponding radio spectra, for convenience. We present, in Section 3.2, the low-frequency part of the dynamic spectrum as it applies to the hectometric Type II event (II(3)). The description of the radio bursts during the early stages of the flare is in Section 3.3. In the next sections, 3.3.1 and 3.3.2, we describe the complex II – III GG-FCII bursts and the decametric stationary Type II in Section 3.4. Lastly we present, briefly, the Type IV continuum in Section 3.5.

3.2. CME – Flare Onset and DH Type II Shock

The event of 20 January 2005 starts with the CME takeoff at 06:33 UT, which accelerates to high sky-plane speed at about 06:54 UT (3242 km sec^{-1} according to Gopalswamy *et al.* (2005) or 2075 km sec^{-1} from Grechnev *et al.* (2008)). The GOES 12 SXR flare onset at 06:36 UT reaches X7.1 intensity at 07:01 – 07:12 UT (Figure 1); its Hα counterpart is a 2B flare from Learmonth (LEAR) at 06:41 – 08:54 with a peak at 06:46 UT. At 06:36 UT the NoRP 3.75 – 35 GHz flux increase starts; this indicates that high-energy electrons were present from the very beginning of the event.

A hectometric Type II event (II(3) in Figure 1) appears at 07:15 UT at 14 MHz on the *Wind*/*Waves* spectra; Pohjolainen *et al.* (2007) calculated the Type II(3) speed from the *Wind*/*Waves* spectra to be in the 750 – 4690 km sec^{-1} range (depending on the selection of the coronal-density model).

Table 1 Overview of the event of 20 January 2005 and associated activity.

Event	UT	Characteristics	Remarks
CME Lift Off	06:33		Gopalswamy *et al.* (2005)
Start	06:36	3.75 – 35.0 GHz	NoRP
SXR Start	06:36	AR 720: N14° W61°	GOES 12
IV Start	06:36	2000 – 100 MHz	ARTEMIS-IV, HiRAS
Narrow-band	06:39	Turnover ≈ 200 MHz	ARTEMIS-IV
J and U		Drifting to ≈ 115 MHz	SAO
Hα Start	06:41	Two ribbon, AR 720	LEAR
HXR increase	06:42	≈ 100 keV	Masson *et al.* (2009)
Spikes Start	06:42:40	450 – 270 MHz	SAO
Continuum Patch	06:43	460 – 350(MHz)	ARTEMIS-IV
(F – H)	to 06:43:45	910 – 690(MHz)	and HiRAS
FCII(1) Start	06:43	650 MHz, 340 km sec^{-1}	ARTEMIS-IV
γ-ray increase	06:43 – 06:44	≈ 780 KeV – 10 MeV	Kurt *et al.* (2010b)
Microwave Peak	06:45	35 GHz	NoRP
γ-ray increase	06:45 – 06:46	≈ 60 – 100 MeV	SONG/CORONAS-F
			Kurt *et al.* (2010b)
II(4) Start	06:45:16	41(F) – 82(H) MHz	ARTEMIS-IV
HXR peak	06:45:30	≈ 100 keV	RHESSI
III(1) GG	06:45:39		ARTEMIS-IV, HiRAS
			and *Wind*/*Waves*
II(1) Start	06:45:39	75(F) – 150(H) MHz 120 km sec^{-1}	ARTEMIS-IV, HiRAS
Release of Electron	06:46 – 06:47	≈ 127 – 225 keV	Grechnev *et al.* (2008)
and Proton		≈ 1.7 GeV	
γ-ray peak	06:46 – 06:47	≈ 300 KeV – 300 MeV	SONG/CORONAS-F
Hα peak	06:46:30	2B	LEAR
II(1) End	06:49	60(F) – 125(H) MHz	ARTEMIS-IV
FCII(1) End	06:52	120 MHz	ARTEMIS-IV
New set of Flare	06:53 – 06:57		TRACE
Kernels activated			(*cf.* Grechnev *et al.*, 2008)
CME First	06:54	PA 293°	LASCO
appearance on C2		3242 km sec^{-1},	Gopalswamy *et al.* (2005)
		or 2075 km sec^{-1}	Grechnev *et al.* (2008)
FCII(2) Start	06:55	650 MHz, 380 km sec^{-1}	ARTEMIS-IV
HXR peak	06:55		RHESSI
(secondary)			Grechnev *et al.* (2008)
Electron release	06:55		Kurt *et al.* (2010b)
Microwave peak	06:55	9.4 GHz	NoRP
(secondary)			
II(2) Start	06:56	100(F) – 200(H) MHz 543 km sec^{-1}	ARTEMIS-IV

Table 1 (*Continued*)

Event	UT	Characteristics	Remarks
III(2) GG	06:57		ARTEMIS-IV, HiRAS and *Wind/Waves*
II(2) End	06:58	75(F) – 150(H) MHz	ARTEMIS-IV
II(4) End	07:02	36(F) – 72 (H) MHz	ARTEMIS-IV
SXR Peak	07:01 – 07:12	X7.1 plateau	GOES 12
FCII(2) End	07:03	120 MHz	ARTEMIS-IV
II(3)	07:15	14 MHz 750 – 4690 km sec^{-1}	*Wind/Waves* Pohjolainen *et al.* (2007)
SXR End	07:26		GOES 12
Hα End	08:54		LEAR

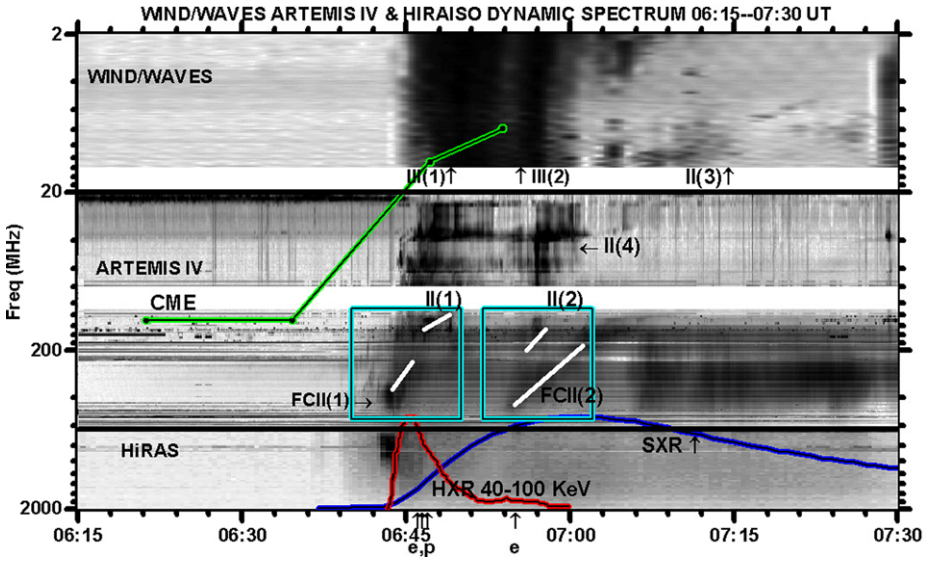

Figure 1 Combined HiRAS, ARTEMIS-IV (ASG), and *Wind/Waves* dynamic spectrum of the event of 20 January 2005, 06:15 – 07:30 UT and 2000 – 2 MHz; the CME trajectory using the Newkirk model (see text) for the height to frequency conversion (green); the GOES SXR flux (blue); the SONG 40 – 100 KeV Channel (red); the two Type II/FCII combinations (II(1)/FCII(1) and II(2)/FCII(2)) are in cyan frames; details are presented in Figure 4. The electron and proton release times as reported by Grechnev *et al.* (2008), Simnett (2007), and Saiz (2005) (Table 1) are annotated with arrows under the plot.

3.3. The Start of Decimetric – Metric Radio Activity

The radio activity commences at the same time with the onset of the SXR flare and the 3.75 – 35 GHz enhancement, at 06:36 UT (Figure 3), with a broad-band Type IV continuum which covers, almost, the combined frequency range (2000 – 20 MHz) of ARTEMIS-IV and HiRAS (Figure 1); its duration extends well past 08:00 UT (Section 3.5).

A little later (06:39 UT), superposed on the continuum, groups of type J and U bursts at decimetric – metric wavelengths appear. Their turnover frequencies drift slowly towards the

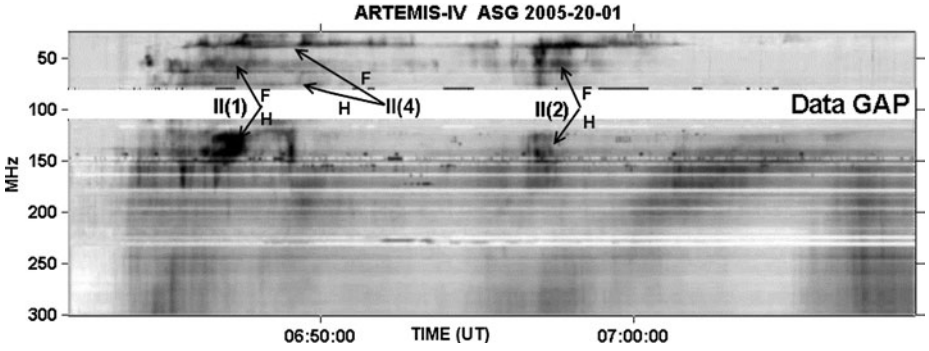

Figure 2 ARTEMIS-IV/ASG dynamic spectrum (linear frequency scale 300 – 40 MHz) of fundamental-harmonic bands of the two metric (II(1) and II(2)) and the decametric (II(4)) shocks.

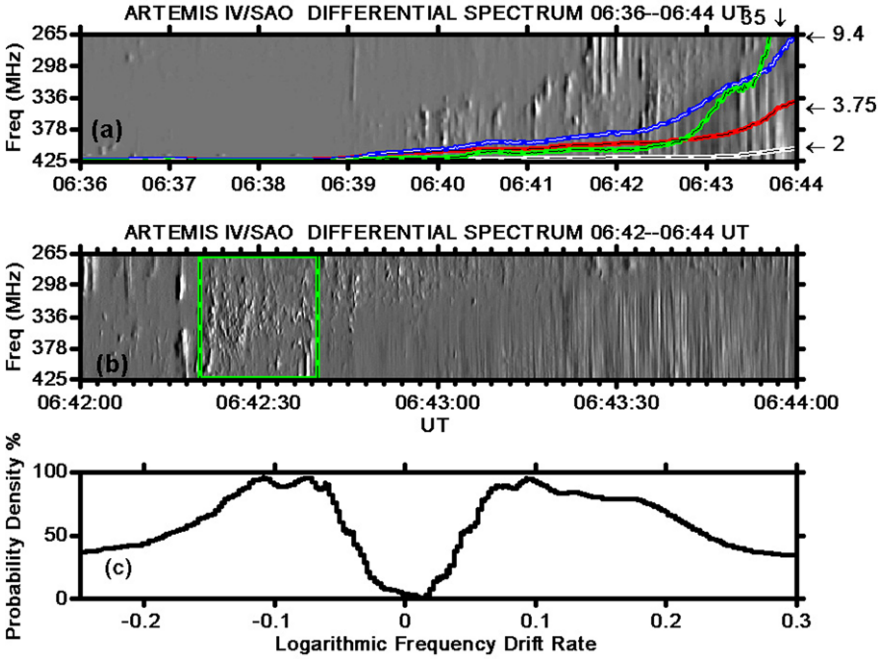

Figure 3 Narrow-band Type III and spikes at high resolution (30 ms) dynamic spectrum; (a) ARTEMIS-IV/SAO and the corresponding NoRPTeX microwave enhancement (frequencies 35.0 (green), 9.4 (blue), 3.75 (red) and 2.2 (white) GHz). This radio activity in the 06:36 – 06:44 UT interval marks the onset of the 20 January 2005 event. (b) ARTEMIS-IV differential spectrum (SAO) in the 06:42 – 06:44 UT interval with 10 msec resolution. On the left, a group of spikes at 06:42:20 UT, marked by the frame, on the right details of the pulsating *patch*. (c) Evolution of average (logarithmic) frequency drift rate ($\mathrm{d}f/f\,\mathrm{d}t$) of the marked spike cluster in the period 06:42:20 – 06:42:40 UT; peaks appear at 0.10, ± 0.06, -0.11 sec^{-1} (Tsitsipis *et al.*, 2006, 2007, also Appendix).

lower part of the spectrum, forming a moving front (Figure 3a). The type J and U bursts are accompanied by groups of narrow-band spikes. After the onset of the 100 KeV HXR at 06:40 UT (Masson *et al.*, 2009) the spike rate increases (06:42:20 – 06:42:40 UT, Figure 3b). The

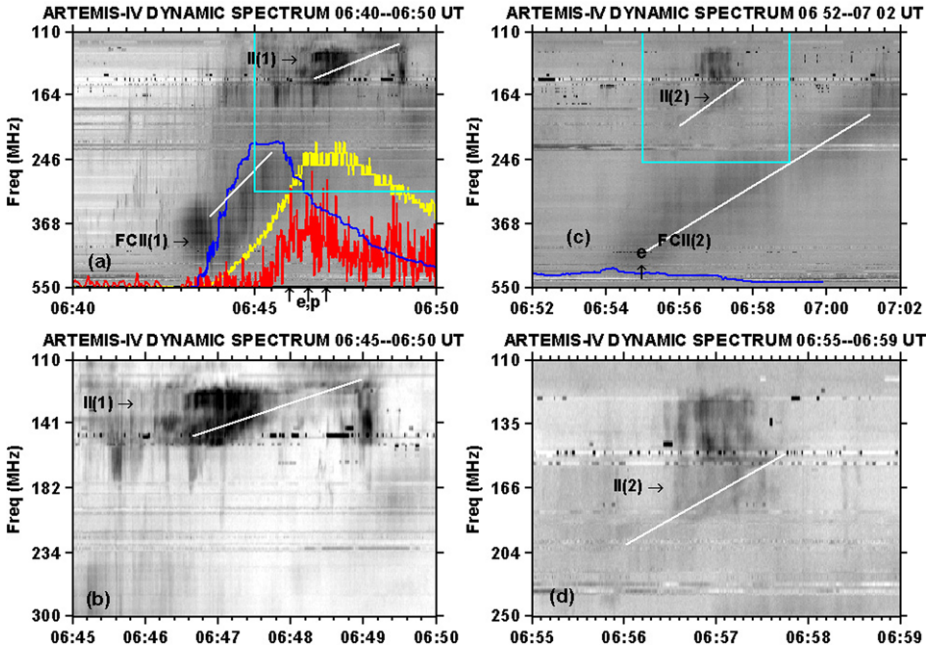

Figure 4 ARTEMIS-IV (ASG) dynamic spectra of the Type II/FCII bursts (see cyan frames on Figure 1); (a) II(1)/FCII(1) 06:40 – 06:50 UT. The electron and proton release times (06:46 – 06:47 UT, Table 1) are marked with arrows under the plot. We have also included SONG/CORONAS-F normalized flux at 40 – 100 KeV (blue), 0.775 – 2.0 MeV (yellow) and 60 – 100 MeV (red). (b) Details of the Type II(1) shock in the 110 – 300 MHz range and the 06:45 – 06:50 UT time interval; it is enclosed by the box in (a). (c) II(2)/FCII(2) 06:52 – 07:02 UT. The electron release time (06:55 UT, Table 1) is marked with an arrow. We have also included SONG/CORONAS-F normalized flux at 40 – 100 Kev (blue). (d) Details of the Type II(2) shock in the 110 – 250 MHz range and the 06:55 – 06:59 UT time interval; it is enclosed by the box in (c).

spikes exhibit a frequency drift rate in the range -100 to 100 MHz sec^{-1} with distinct peaks at ± 0.06 sec^{-1}, ± 0.10 sec^{-1} corresponding to exciter speeds in the 10 – 16 Mm sec^{-1} range (Figure 3c). The Type III(J) bursts and the spikes, mentioned above, possibly mark an additional acceleration episode, corresponding to a small peak on the NoRP recordings. At 06:43:00 – 06:43:45 UT a continuum patch appears on the dynamic spectra in the frequency range 1000 – 760 MHz (H) and 475 – 350 MHz (F) (Figure 1). The continuum patch exhibits a pulsating structure (Figure 3) with periodic behaviour (0.32 Hz: main FFT peak, 10 Hz: secondary FFT peak) and coincides with the onset of the flare continuum FCII(1).

3.3.1. The first Type II – FCII – III GG Complex Burst

A close examination of FCII(1) (Figure 5) reveals extended groups of Type III bursts and reverse-drift Type III bursts sharing a common onset frequency, which corresponds to the separation frequency of the bidirectional Type III bursts. The onset frequency drifts towards lower frequencies. The high-frequency part of the FCII(1) (270 – 450 MHz) was recorded by the ARTEMIS-IV/SAO with high time resolution (100 sec^{-1}). This part was examined using the methodology introduced by Tsitsipis *et al.* (2006, 2007), which provides statistics on the frequency drift rate based on a 2D FFT of the dynamic spectrum (see Appendix). The

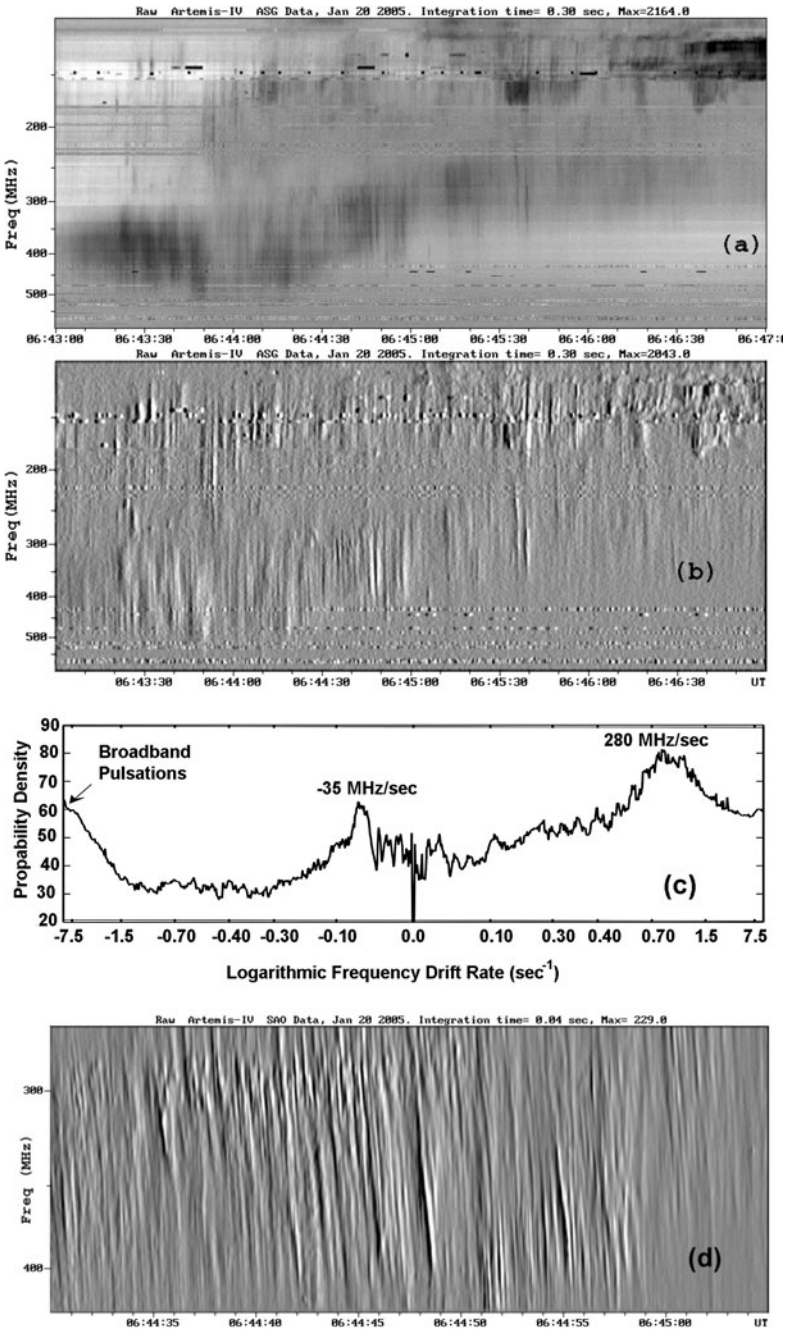

Figure 5 ARTEMIS-IV Spectra of II(1)/FCII(1), *bidirectional* Type III and reverse-drift Type III-like bursts; (a) ASG dynamic spectrum (06:43 – 06:47 UT) (b) ASG differential spectrum, (c) evolution of average (logarithmic) frequency drift rate ($\mathrm{d}f/f\,\mathrm{d}t$) of the lowerpart of the differential spectrum (06:44 – 06:46 UT and 450 – 300 MHz) (Appendix) with peaks at -0.10 sec^{-1} (20 Mm sec^{-1} outbound) and 0.83 sec^{-1} ($\approx$ 120 Mm sec^{-1} reverse drift); we have assumed radial propagation and a twofold Newkirk density – height coronal model. (d) SAO differential spectrum 06:44:30 – 06:45:05 UT.

logarithmic frequency drift rates peak at -0.10 sec^{-1} and 0.17 sec^{-1} MHz sec^{-1} (speeds 15 – 20 Mm sec^{-1}). A third and more pronounced peak at 0.83 sec^{-1} is characteristic of the reverse-drift Type IIIs. For the twofold Newkirk model, the exciter speed is estimated to $\approx$ 120 Mm sec^{-1}.

The Type II event (II(1) in Figure 4a and 4b) appeared on the ARTEMIS-IV recordings at $\approx$ 06:45:40 UT and 145 MHz, ending at 06:49 UT and 125 MHz. The radial shock speed, as calculated from the twofold Newkirk coronal model, was found to be quite small ($\approx$ 120 km sec^{-1}).

The II(1), FCII(1), and III(1) combination of bursts appears to be associated with the rise phase of the SXR flare (Figure 1). The intense Type III GG (III(1) in Figure 1) at 06:45:39 UT spans the whole range of the combined HiRAS – ARTEMIS-IV – *Wind*/*Waves* spectra, and it coincides in time with the particle release and the HXR – γ-microwave peaks as specified in the following paragraph.

The rise in microwave and 100 keV HXR flux (HXR enhancement starts at 06:40 UT, peak at $\approx$ 06:45:30 UT) overlaps in time with the drift of FCII(1) ($\approx$ 340 km sec^{-1}) to lower frequencies (6:44 – 6:46 UT), as it tends to converge with II(1), on the dynamic spectra, near 200 MHz ($\approx$ 0.26 $R_{\odot}$, Figures 1 and 4a). This FCII(1) – II(1) convergence coincides with a sharp increase of the γ-ray flux around 6:45 – 6:46 UT. The latter originates from pion decay, as protons with energies in excess of 300 MeV interact with nuclei in the ambient corona, the pion decay time being $\approx$ 06:45 UT (Kuznetsov *et al.*, 2008; Grechnev *et al.*, 2008). The pion decay emission supports the path and time-of-flight calculations of Grechnev *et al.* (2008), which provide an estimate of the proton release in the 06:46 – 06:47 UT interval. The electron release is estimated within the same interval as the pion decay, and the HXR bremsstrahlung light curves present similar profiles.

3.3.2. The Second Type II – FCII – III GG Complex Burst

Another Type II occurrence (II(2) in Figures 1, 4c and 4d) starts at 06:56 and 200 MHz, drifting at $\approx$ 543 km sec^{-1}. It is accompanied by the FCII(2) event (starting 06:55 UT), which consists mainly of a group of reverse-drift Type III events, with a total drift towards low frequencies corresponding to a radial exciter speed $\approx$ 380 km sec^{-1}. It also coincides with a secondary maximum of the HXR (Grechnev *et al.*, 2008, their Figure 5) associated with microwave flux enhancement, after 6:53 UT; to these correspond an electron release at $\approx$ 06:55 UT and the second DH Type III GG (III(2)), starting, on the dynamic spectrum, from the Type II(2) lane. This Type II event originated, probably, from a flare blast wave.

The complex II(2)/FCII(2) burst is associated with the maximum of the SXR flux but also with a weak HXR, compared to the previous bursts, and a microwave peak.

3.4. The Stationary Decametric Type II

The Stationary Decametric Type II event starts at 06:45:16 UT at 41 MHz (Fundamental), exhibiting a fundamental – harmonic structure; it is labeled II(4) in Figures 1 and 2. The harmonic structure is not very well defined as it overlaps, somewhat, with the fundamental of II(2) and it coincides, also, in frequency with the ARTEMIS-IV data gap. It ends at about 07:02 UT after the secondary energy release and the injection of the second Type III group (III(2)). A number of Type III bursts appear to originate from the Type II band; they merge into the two III GG groups (III(1) and III(2)).

3.5. The Type IV Continuum

The Type IV burst becomes more pronounced after II(2)/FCII(2); it exhibits rich fine structure too, which includes broad-band pulsations, intermediate drift bursts (fibers), and a variety of narrow-band bursts.

Between FCII(2) and the stationary Type IV a cluster of narrow-band structures, mostly Type III, were recorded by ARTEMIS-IV/SAO at 300 – 400 MHz. A little after 07:00 UT, Grechnev *et al.* (2008) observed an expanding arcade, on GOES/SXI and EUV (SOHO/EIT) images, which may be the source of the IV event.

4. Summary and Discussion

We have presented a radio signature analysis of the solar eruptive event of 20 January 2005 and we have studied the association of the radio bursts with the energy release and the active phenomena comprising this event.

4.1. The Dynamic Spectrum of 20 January 2005

The two different Type II bursts (II(1) and II(2)) exhibited significantly different drift rates and were well separated in time; and each was associated with an HXR peak. This suggests distinct shocks.

The first of them, II(1), was preceded by metric – decimetric drifting structures such as isolated Type III(J) and III(U) burst spikes and narrow-band Type III events (mostly with reverse slope); these can be identified as the signature of reconnection and electron acceleration episodes above expanding soft X-ray loops (Klassen, Pohjolainen, and Klein, 2003). Furthermore, the J – U bursts, at the beginning of the metric radio event, trace the initial closed magnetic structure.

Both II(1) and II(2) are accompanied by a flare continuum (FCII(1) and FCII(2), respectively) which, on close examination, consists of bidirectional and reverse-drift Type III elements; these continua also trace electrons accelerated in reconnection sites. The drift rate of the FCII suggests outward movement of the reconnection.

The large Type III groups, III(1) and III(2), appear to start, in part, from the Type II bands (II(1) and II(2), respectively) and in part from the decametric shock II(4) as discussed in Section 3.4. A few start at higher frequencies; this indicates shock acceleration of a significant part of the electrons, exciting the Type III events. Prior to the III GGs, the Type III(J) or III(U) bursts trace energetic electrons that are confined and do not access interplanetary space. The continuation of III(1) and III(2) into hectometric frequencies implies an opening of initially closed magnetic lines and the escape of energetic particles into interplanetary space. This agrees with Masson *et al.* (2009), as they report, before III(1), a number of acceleration episodes in HXR, of which the first few do not have DH radio signatures. Within this context, the III(1) and III(2) onsets are consistent with the energetic-particle release times.

4.2. Acceleration and Release of Energetic Particles within the Framework of the Standard Flare – CME Model

The three main categories of particle acceleration processes (see, *e.g.*, Anastasiadis, 2002; Aschwanden, 2008, for a review) in solar flares and CMEs (electric DC-field acceleration

at magnetic X-points, stochastic acceleration by turbulence, and MHD shock acceleration in reconnection outflows) are all present in the extreme event of 20 January 2005. The DC-field acceleration appears in a reconnecting current sheet driven by the rising CME. The other two processes operate in the reconnection outflow termination shock accelerating the highly energetic, electron and proton populations (Mann, Aurass, and Warmuth, 2006; Mann, Warmuth, and Aurass, 2009; Warmuth, Mann, and Aurass, 2009).

A close association, in time, of the electron injection at ≈06:45:40 UT, the HXR primary peak, and the start of the III GG burst (III(1)) was established in Section 3.3.1. The convergence of II(1) – FCII(1) spectra (06:45 – 06:47 UT), on the other hand, coincides with the estimated time of proton escape at ≈06:45:30 (Grechnev *et al.*, 2008) as stated in Section 4.1. This temporal association seems to indicate that II(1) may be a termination shock formed as the reconnection front, FCII(1), rises; on the other hand the expanding flare loops may *piston drive* II(1) as a flare blast (Vršnak and Cliver, 2008). In both cases this shock formation may be accompanied by particle acceleration and release. What weighs more in favour of II(1) as a flare-associated Type II event is the appearance, in the decametric frequency range, of II(4) whose spectrum appears to be more typical of a zero-drift termination shock; this also accelerates a significant part of the Type III bursts in the groups III(1) and III(2).

In an attempt to introduce a model interpreting the observational data and the evolution of the event, we firstly invoke CME-driven reconnection as proposed by Forbes and Lin (2000), Forbes (2003), and Priest and Forbes (2002); the rising CME stretches and deforms the coronal magnetic-field lines resulting in a vertical current sheet, where magnetic reconnection commences. Since X-type reconnection is directly associated with counter-streaming electron beams appearing as bidirectional Type IIIs (Aschwanden *et al.*, 1995; Aschwanden and Benz, 1997) the FCII(1) is interpreted as a moving reconnection front within the framework of this mechanism (Figure 6).

Kliem, Karlický, and Benz (2000) interpret pulsating structures such as the continuum patch marking the start of FCII(1) in terms of quasi-periodic particle acceleration episodes. These originate from a magnetic reconnection in large-scale current sheets and are characterized by repeated formation and coalescence of magnetic islands, feeding a continuously growing plasmoid, which drifts outwards in the corona. In this case, however, there are no further observational signatures of a rising plasmoid.

The slowly drifting burst II(4) may be a reconnection outflow termination shock as proposed by Aurass, Vršnak, and Mann (2002) and Aurass *et al.* (2003). The only difference is that they envisage a shock formed below the X-reconnection as the outflow encounters the post-flare loop tops; our data, however, suggest that the shock is above the reconnection as the Type II(4) is in the decametric range and always is at lower frequencies than the FCII(1). Therefore, we conclude that the shock may be formed from the upper outflow (Figure 6). The reconnection outflow termination shock was found to be capable of accelerating the highly energetic electron and proton populations indicated in the SONG recordings (Mann, Aurass, and Warmuth, 2006; Mann, Warmuth, and Aurass, 2009; Warmuth, Mann, and Aurass, 2009). The presence of II(1) complicates the spectral form somewhat; however, it may originate at the flanks of the rising flare loops. Hence it has a rather small speed.

The difficulties of the detection of the reconnection outflow termination shock on the top of the post-flare loops are attributed by Aurass, Vršnak, and Mann (2002) to confusion on the dynamic spectra due to other radio bursts, especially during the impulsive phase of the flare.

On the left of Figure 6 we propose a model including both CME-induced reconnection (Forbes, 2003) and termination shocks from reconnection outflow jets (Aurass, Vršnak,

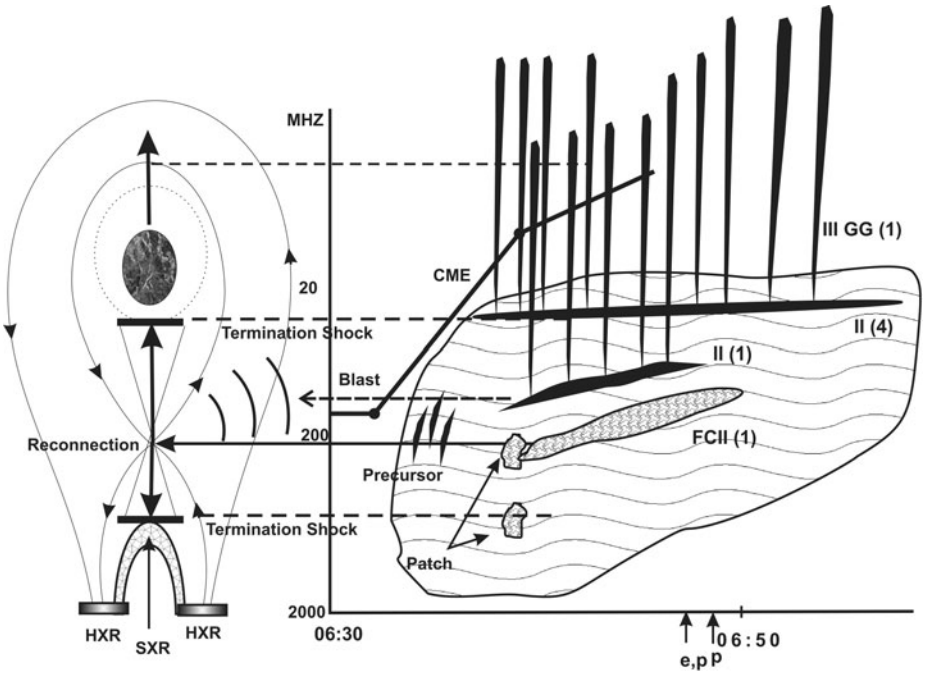

Figure 6 Comparison of the standard CME – flare model with the combined HiRAS, ARTEMIS-IV (ASG) and *Wind*/*Waves* dynamic spectrum. On the left we present the CME-induced reconnection (Forbes, 2003) supplemented with the reconnection outflow jets and the corresponding termination shocks (Aurass, Vršnak, and Mann, 2002) where the upward shock appears after the CME. An additional Type II event originating from the flare-loop expansion moves sideways. On the right we present the dynamic spectrum resulting from this process.

and Mann, 2002); the combined mechanisms may interpret the dynamic spectrum which we have included on the right of the figure for comparison. At this point we note that the II(1)/FCII(1)/III(1) complex burst was preceded by Type III(J) and Type III(U) bursts, spikes, and the start of the Type IV continuum. This indicates that energetic electrons were present before the onset of the main part of the energy release in the flare, probably originating in the early stages of the reconnection process.

During the second release of electrons, manifest as III(2) and associated with the secondary HXR peak reported by Grechnev *et al.* (2008), it is expected that the acceleration region has moved higher as this HXR peak is quite small. The Type II burst (II(2)) drifts at ≈ 540 km sec^{-1} and, being far from the CME, may be interpreted as a flare blast at this point. The whole Type II – flare continuum complex (II(2) – FCII(2)) follows the ignition of the, so far inactive, flare kernels (Section 3.3.2). Grechnev *et al.* (2008) studied the TRACE 1600 Å images during the time interval 6:52:41 – 6:57:30 UT, marked four pairs of kernels and computed intensity – time profiles of their brightness. As the brightness for two pairs of kernels decreases it increases, on the other two; this transition appears at about 6:53 – 6:54 UT. We note, at this point, that the decametric shock, II(4), is still present until 07:02 UT, which is almost coincident with the end of the II(2)/FCII(2) burst. This relatively long duration of the termination shock radio burst has already been reported by Aurass (2003).

5. Conclusions

The present study was based on high cadence data from the ARTEMIS-IV solar radiospectrograph in the 650 – 20 MHz range, extended, as regards the frequency range, with HiRAS (25 – 2500 MHz) and *Wind*/*Waves* (13.825 – 1.075 MHz, 1040 – 20 kHz) recordings and supplemented with NoRP (2 – 35 GHz), SONG (0.03 – 100 MeV), and GOES data; they were compared with the energetic-particle release times reported in the literature. This made possible a multi-frequency and multi-instrument study of different aspects of the active phenomena in the 20 January 2005 event. Our analysis was focused on the *radio perspective* of the event, as radio observations provide a rich collection of diverse diagnostics in the study of the shock-formation processes, the particle acceleration, and the mass ejection from the Sun. The results were interpreted in terms of the standard CME – flare model, which applies to eruptive flares and invokes the CME-induced reconnection scenario.

A number of particle accelerators were identified, and their relative importance in the manifestation of the event was tested against their radio signatures. Firstly the CME-associated shock acceleration seems to be of little importance. The reconnection in the wake of the CME and the reconnection outflow termination shocks (both above and below the reconnection) appear to be the main contributors of energetic electrons and protons.

The results are consistent with the standard CME – flare model with the reconnection outflow termination shocks and the reconnecting current sheet in the wake of the CME as sources of energetic particles.

Acknowledgements We appreciate discussions and assistance of K.-L. Klein and C. Caroubalos and C. Alissandrakis, the availability of the Nobeyama Radio Polarimeter data due to H. Nakajima and of the SONG recordings due to B.Yu. Yushkov. We also thank the anonymous referees for their comments and suggestions on the draft, which have substantially improved the quality of this report. This work was supported in part by the University of Athens Research Center (ELKE/EKPA).

Appendix: Detection and Statistical Analysis of Quasi-Linear Structures Embedded in Complex Dynamic Spectra

In the study of solar radio bursts, various types of structures often appear on the dynamic spectra intertwined, overlapping, disturbed by terrestrial signals, and embedded in a continuum background. A methodology (Tsitsipis *et al.*, 2006, 2007) for the detection and statistical analysis of linear structures has been developed and is presented here in brief.

The continuous background is eliminated by means of high-pass filtering; this suppresses slowly varying components enhancing fine structure with fast temporal variation. The terrestrial interference appears in the form of lines parallel to the temporal axis and may be suppressed with directional filtering.

In the resulting clean dynamic spectrum, all frequency channels are normalized to the same minimum and maximum; this eliminates variations of brightness along the frequency axis which may interfere with the subsequent processing algorithms.

For the statistical analysis of quasi-linear structures representing Type III events, fibers, pulsations *etc.* on the dynamic spectra, we introduce the concept of energy density as a function of angle which measures the signal power of a 2D image (a dynamic spectrum in this case) along a certain direction. In terms of the two-dimensional Fourier transform of the dynamic spectrum:

$$F(\xi_1, \xi_2) = \int_{-\infty}^{\infty} \int_{-\infty}^{\infty} f(x, y) \cdot \mathrm{e}^{-\mathrm{j}2\pi(x\xi_1 + y\xi_2)} \, \mathrm{d}x \, \mathrm{d}y. \tag{A.1}$$

The energy density as a function of angle (angular energy density) is defined as

$$S(\theta) = 2 \int_0^\infty \left| F(\xi, \theta) \right|^2 \xi \, \mathrm{d}\xi. \tag{A.2}$$

This exhibits local maxima at the points where θ equals the slopes of linear or quasi-linear segments within the image, yet it is not affected by their position within it. These peaks of energy per direction on the image indicate, in a statistical sense, the dominant slopes of linear or quasi-linear segments within the image; or, in this case, the peaks of frequency drift rates which may be interpreted as the dominant exciter velocities once a coronal density – height model has been adopted. An example of the usage of this method appears in Section 3.3 and in Figure 5 (panels (c) and (e)), where we present the statistics of the frequency drift rates.

References

Anastasiadis, A.: 2002, *J. Atmos. Solar Terr. Phys.* **64**, 481.
Aschwanden, M.J.: 2008, *J. Astrophys. Astron.* **29**, 3.
Aschwanden, M.J., Benz, A.O.: 1997, *Astrophys. J.* **480**, 825.
Aschwanden, M.J., Benz, A.O., Dennis, B.R., Schwartz, R.A.: 1995, *Astrophys. J.* **455**, 347.
Aurass, H.: 2003, *Hvar Obs. Bull.* **27**, 103.
Aurass, H., Vršnak, B., Mann, G.: 2002, *Astron. Astrophys.* **384**, 273.
Aurass, H., Klein, K.L., Zlotnik, E.Y., Zaitsev, V.V.: 2003, *Astron. Astrophys.* **410**, 1001.
Aurass, H., Mann, G., Rausche, G., Warmuth, A.: 2006, *Astron. Astrophys.* **457**, 681.
Bastian, T.S., Pick, M., Kerdraon, A., Maia, D., Vourlidas, A.: 2001, *Astrophys. J. Lett.* **558**, L65.
Bazilevskaya, G.A.: 2009, *Adv. Space Res.* **43**, 530.
Belov A.V.e.: 2005, In: Sripathi Acharya, B., Gupta, S., Jagadeesan, P., Jain, A., Karthikeyan, S., Morris, S., Tonwar, S. (eds.) *Proceedings of the 29th Internat. Cosmic Ray Conf.* **1**, *TIFR*, *Mumbai*, 189.
Benz A.O.: 2003, In: Klein, L. (ed.) *Energy Conversion and Particle Acceleration in the Solar Corona*, *Lecture Notes in Physics* **612**, Springer, Berlin, 80.
Bougeret, J.L., Kaiser, M.L., Kellogg, P.J., Manning, R., Goetz, K., Monson, S.J., Monge, N., Friel, L., Meetre, C.A., Perche, C., Sitruk, L., Hoang, S.: 1995, *Space Sci. Rev.* **71**, 231.
Caroubalos, C., Maroulis, D., Patavalis, N., Bougeret, J.L., Dumas, G., Perche, C., Alissandrakis, C., Hillaris, A., Moussas, X., Preka-Papadema, P., Kontogeorgos, A., Tsitsipis, P., Kanelakis, G.: 2001, *Exp. Astron.* **11**, 23.
Claßen, H.T., Aurass, H.: 2002, *Astron. Astrophys.* **384**, 1098.
Crosby, N.B.: 2009, *Adv. Space Res.* **43**, 559.
Faindberg, J., Stone, R.G.: 1970, *Solar Phys.* **15**, 433.
Forbes, T.G.: 2003, *Adv. Space Res.* **32**, 1043.
Forbes, T.G., Lin, J.: 2000, *J. Atmos. Solar Terr. Phys.* **62**, 1499.
Goldman, M.V.: 1983, *Solar Phys.* **89**, 403.
Gopalswamy N., Xie H., Yashiro S., Usoskin I.: 2005, In: Sripathi Acharya, B., Gupta, S., Jagadeesan, P., Jain, A., Karthikeyan, S., Morris, S., Tonwar, S. (eds.) *Proceedings of the 29th Internat. Cosmic Ray Conf.* **1**, *TIFR*, *Mumbai*, 169.
Grechnev, V.V., Kurt, V.G., Chertok, I.M., Uralov, A.M., Nakajima, H., Altyntsev, A.T., Belov, A.V., Yushkov, B.Y., Kuznetsov, S.N., Kashapova, L.K., Meshalkina, N.S., Prestage, N.P.: 2008, *Solar Phys.* **252**, 149.
Kahler, S., Sheeley, N.R. Jr., Howard, R.A., Michels, D.J., Koomen, M.J.: 1984, *Solar Phys.* **93**, 133.
Klassen, A., Pohjolainen, S., Klein, K.L.: 2003, *Solar Phys.* **218**, 197.
Klein, K., Krucker, S., Lointier, G., Kerdraon, A.: 2008, *Astron. Astrophys.* **486**, 589.
Klein, K., Mouradian, Z.: 2002, *Astron. Astrophys.* **381**, 683.
Kliem, B., Karlický, M., Benz, A.O.: 2000, *Astron. Astrophys.* **360**, 715.
Kliem B., MacKinnon A., Trottet G., *et al.*: 2003, In: Klein, L. (ed.) *Energy Conversion and Particle Acceleration in the Solar Corona*, *Lecture Notes in Physics* **612**, Springer, Berlin, 263.
Kondo, T., Isobe, T., Igi, S., Watari, S., Tokumaru, M.: 1995, *J. Commun. Res. Lab.* **42**, 111.
Kontogeorgos, A., Tsitsipis, P., Caroubalos, C., Moussas, X., Preka-Papadema, P., Hilaris, A., Petoussis, V., Bouratzis, C., Bougeret, J.L., Alissandrakis, C.E., Dumas, G.: 2006, *Exp. Astron.* **21**, 41.
Kurt, V.G., Logachev, I.I., Pissarenko, N.F.: 1977, *Solar Phys.* **53**, 157.

Kurt, V.G., Svertilov, S.I., Yushkov, B.Y., Bogomolov, A.V., Grechnev, V.V., Galkin, V.I., Bogomolov, V.V., Kudela, K., Logachev, Y.I., Morozov, O.V., Myagkova, I.N.: 2010, *Astron. Lett.* **36**, 280.
Kurt, V.G., Yushkov, B.Y., Kudela, K., Galkin, V.I.: 2010, *Cosm. Res.* **48**, 70.
Kuznetsov S.N., Kurt V.G., Yushkov B.Y., *et al.*: 2008, In: Caballero, R., D'Olivo, J., Medina-Tanco, G., Nellen, L., Sanchez, F., Valdes-Galicia, J. (eds.) *Proceedings of the 30th Internat. Cosmic Ray Conf.* **1**, 121.
Kuznetsov, S.N., Kurt, V.G., Yushkov, B.Y., Myagkova, I.N., Kudela, K., Kaššovicová, J., Slivka, M.: 2006, *Contrib. Astron. Obs. Skaln. Pleso* **36**, 85.
Kuznetsov V.D.: 2004, In: Stepanov, A.V., Benevolenskaya, E.E., Kosovichev, A.G. (eds.) *Multi-Wavelength Investigations of Solar Activity*, *IAU Symposium* **223**, Cambridge University Press, Cambridge, 693.
Lin, R.P., Evans, L.G., Fainberg, J.: 1973, *Astrophys. Lett.* **14**, 191.
Maia, D., Pick, M., Vourlidas, A., Howard, R.: 2000, *Astrophys. J. Lett.* **528**, L49.
Mann, G., Aurass, H., Warmuth, A.: 2006, *Astron. Astrophys.* **454**, 969.
Mann, G., Warmuth, A., Aurass, H.: 2009, *Astron. Astrophys.* **494**, 669.
Masson, S., Klein, K.L., Bütikofer, R., Flückiger, E., Kurt, V., Yushkov, B., Krucker, S.: 2009, *Solar Phys.* **257**, 305.
Mavromichalaki, H.: 2009, *Adv. Space Res.* **43**, 467.
Nakajima, H., Sekiguchi, H., Sawa, M., Kai, K., Kawashima, S.: 1985, *Publ. Astron. Soc. Japan* **37**, 163.
Newkirk, G.J.: 1961, *Astrophys. J.* **133**, 983.
Nindos A., Aurass H.: 2007, In: Klein, K.-L., MacKinnon, A. L. (eds.) *The High Energy Solar Corona: Waves, Eruptions, Particles*, *Lecture Notes in Physics* **725**, Springer, Berlin, 251.
Pick, M., Vilmer, N.: 2008, *Astron. Astrophys. Rev.* **16**, 1.
Pick, M., Forbes, T.G., Mann, G., Cane, H.V., Chen, J., Ciaravella, A., Cremades, H., Howard, R.A., Hudson, H.S., Klassen, A., Klein, K.L., Lee, M.A., Linker, J.A., Maia, D., Mikic, Z., Raymond, J.C., Reiner, M.J., Simnett, G.M., Srivastava, N., Tripathi, D., Vainio, R., Vourlidas, A., Zhang, J., Zurbuchen, T.H., Sheeley, N.R., Marqué, C.: 2006, *Space Sci. Rev.* **123**, 341.
Plainaki, C., Belov, A., Eroshenko, E., Mavromichalaki, H., Yanke, V.: 2007, *J. Geophys. Res.* **112**(11), 4102.
Pohjolainen, S., Hori, K., Sakurai, T.: 2008, *Solar Phys.* **253**, 291.
Pohjolainen, S., van Driel-Gesztelyi, L., Culhane, J.L., Manoharan, P.K., Elliott, H.A.: 2007, *Solar Phys.* **244**, 167.
Priest, E.R., Forbes, T.G.: 2002, *Astron. Astrophys. Rev.* **10**, 313.
Robinson, R.D.: 1978a, *Aust. J. Phys.* **31**, 533.
Robinson, R.D.: 1978b, *Solar Phys.* **60**, 383.
Robinson, R.D.: 1985, In: McLean, D.J., Labrum, N.R. (eds.) *Solar Radiophysics: Studies of Emission from the Sun at Metre Wavelengths*, Cambridge University Press, Cambridge, 385.
Saiz, A.e.: 2005, In: Sripathi Acharya, B., Gupta, S., Jagadeesan, P., Jain, A., Karthikeyan, S., Morris, S., Tonwar, S. (eds.) *Proceedings of the 29th Internat. Cosmic Ray Conf.* **1**, *TIFR*, *Mumbai*, 229.
Simnett, G.M.: 2007, *Astron. Astrophys.* **472**, 309.
Temmer, M., Veronig, A.M., Kontar, E.P., Krucker, S., Vršnak, B.: 2010, *Astrophys. J.* **712**, 1410.
Tsitsipis, P., Kontogeorgos, A., Hillaris, A., Moussas, X., Caroubalos, C., Preka-Papadema, P.: 2007, *Pattern Recognit.* **40**(2), 563.
Tsitsipis P., Kontogeorgos A., Moussas X., Preka-Papadema P., Hillaris A., Petoussis V., Caroubalos C., Alissandrakis C.E., Bougeret J.L., Dumas G.: 2006, In: Solomos, N. (ed.) *Recent Adv. Astron. Astroph.* **CS-848**, Am. Instit. Phys., New York, 874.
Vashenyuk E.V.e.: 2005, In: Sripathi Acharya, B., Gupta, S., Jagadeesan, P., Jain, A., Karthikeyan, S., Morris, S., Tonwar, S. (eds.) *Proceedings of the 29th Internat. Cosmic Ray Conf.* **1**, *TIFR*, *Mumbai*, 209.
Vršnak, B., Cliver, E.W.: 2008, *Solar Phys.* **253**, 215.
Vršnak, B., Magdalenić, J., Aurass, H.: 2001, *Solar Phys.* **202**, 319.
Warmuth, A., Mann, G., Aurass, H.: 2009, *Astron. Astrophys.* **494**, 677.
Wild, J.P., Smerd, S.F., Weiss, A.A.: 1963, *Ann. Rev. Astron. Astrophys.* **1**, 291.